

# Synthesis, Reactivity, and Electronic Structure of a Bioinspired Heterobimetallic $[\text{Ni}(\mu\text{-S}_2)\text{Fe}]$ Complex with Disulfur Monoradical character

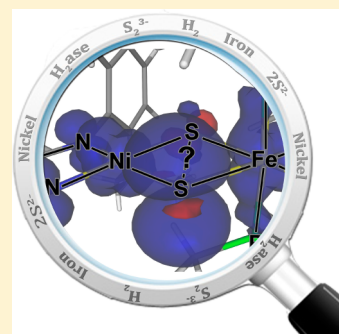
Robert Rudolph,<sup>†</sup> Burgert Blom,<sup>†</sup> Shenglai Yao,<sup>†</sup> Florian Meier,<sup>‡</sup> Eckhard Bill,<sup>§</sup> Maurice van Gastel,<sup>§</sup> Nils Lindenmaier,<sup>†</sup> Martin Kaupp,<sup>\*,‡</sup> and Matthias Driess<sup>\*,†</sup>

<sup>†</sup>Department of Chemistry, Metalorganics and Inorganic Materials Sekr. C2, and <sup>‡</sup>Department of Chemistry, Theoretical Chemistry Sekr. C7, Technische Universität Berlin, Strasse des 17. Juni 135, D-10623 Berlin, Germany

<sup>§</sup>Max Planck Institute for Chemical Energy Conversion, Stiftsstrasse 34-36, D45470 Mülheim/Ruhr, Germany

## Supporting Information

**ABSTRACT:** The first synthesis of a monoradical  $\text{Ni}(\mu\text{-S}_2)\text{Fe}$  core in the  $[(\text{Nacnac})\text{Ni}(\mu\text{-S}_2)\text{Fe}(\text{dmpe})_2]$  complex **3** could be accomplished in good yields by  $\text{PMe}_3$  elimination from the zerovalent iron complex  $[(\text{dmpe})_2(\text{PMe}_3)\text{Fe}]$  (**2**;  $\text{dmpe} = 1,2\text{-bis}(\text{dimethylphosphine})\text{-ethane}$ ) upon reaction with the supersulfido nickel(II) complex  $[(\text{Nacnac})\text{Ni}(\text{S}_2)]$  (**1**;  $\text{Nacnac} = \text{CH}\{(\text{CMe})(2,6\text{-}i\text{Pr}_2\text{C}_6\text{H}_3\text{N})\}_2$ ). Complex **3** bears Ni(II) and Fe(II) centers, both of which are in a low-spin state. A single electron is located in the HOMO and is somewhat delocalized over the  $\text{Ni}(\mu\text{-S}_2)\text{Fe}$  core, so that the bridging disulfur subunit exhibits some “subulfide”  $\text{S}_2^{3-}$  character. Compound **3** represents a bioinspired example of a monoradical with a  $\text{Ni}(\mu\text{-S}_2)\text{Fe}$  structural motif, reminiscent of the  $\text{Ni}(\mu\text{-S}_2)\text{Fe}$  core structure of the active site in  $[\text{NiFe}]$  hydrogenases. Its oxidation with  $[\text{Fe}(\eta^5\text{-C}_5\text{H}_5)_2][\text{B}(\text{C}_6\text{H}_3(\text{CF}_3)_2)_4]$  affords the product  $[(\text{Nacnac})\text{Ni}(\mu\text{-S})\text{Fe}(\text{dmpe})_2][\text{B}(\text{C}_6\text{H}_3(\text{CF}_3)_2)_4]$  (**4**), and complex **3** can alternatively be prepared via a reductive route upon reaction of  $[\text{Co}(\eta^5\text{-C}_5\text{Me}_5)_2][(\text{Nacnac})\text{-NiS}_2]$  (**6**) with the Fe(0) precursor **2**. All synthesized complexes were fully characterized, including in some cases single-crystal X-ray diffraction analysis, magnetometry, EPR, NMR, and  $^{57}\text{Fe}$  Mössbauer spectroscopy. DFT calculations were used to compute the spectroscopic parameters and to establish the electronic structure of **3** and its oxidized and reduced forms and related complexes.

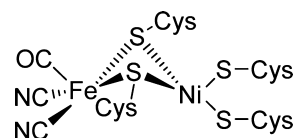


## INTRODUCTION

Nickel–iron–sulfur clusters are one of the most important structural motifs found in nature,<sup>1</sup> and their existence has even been implicated in the geochemical theory of the origin of life on earth.<sup>2</sup> Cubane-type  $\text{NiFe}_3\text{S}_4$  clusters, for example, are crucial in  $\text{CO}_2$  fixation in acetyl-CoA synthase,<sup>3</sup> and several synthetic models have been reported, particularly by Holm and co-workers.<sup>4</sup> Nickel–iron–sulfur clusters of lower nuclearity, particularly those of the type  $\text{NiFeS}_2$ , are also crucial in biology and are exemplified by the  $[\text{NiFe}]$  hydrogenases.<sup>5</sup> Hydrogenases, which are responsible for the reversible conversion of hydrogen for energy conversion by several microorganisms, can further be subclassified through their active sites, and three classes of hydrogenases have emerged in the last decades: the bimetallic  $[\text{NiFe}]$  and  $[\text{FeFe}]$  and the monometallic  $[\text{Fe}]$  hydrogenases.<sup>6</sup> Numerous synthetic models of the  $[\text{FeFe}]$  hydrogenases have been reported,<sup>7,8</sup> while the development of a  $[\text{NiFe}]$  hydrogenase mimic is more challenging, and to date only a few functional examples are known. The active site of the  $[\text{NiFe}]$  hydrogenase was structurally elucidated nearly 20 years ago by X-ray diffraction analysis of *Desulfovibrio gigas*.<sup>9</sup> This study revealed four sulfur-bound cysteine residues coordinated to a nickel core, two of which are terminally bound to the nickel

center and the remaining two of which are bridged to the  $\text{Fe}(\text{CN})_2(\text{CO})$  site (Chart 1).

**Chart 1.** Active Site of  $[\text{NiFe}]$  Hydrogenase Identified by X-ray Diffraction Analysis of the Active Site of Bacteria *Desulfovibrio gigas*<sup>a</sup>



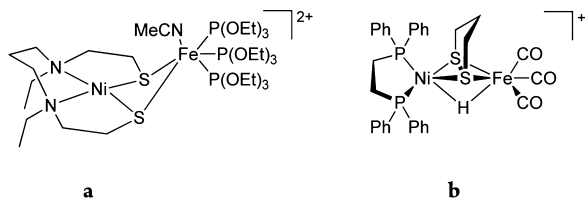
<sup>a</sup>Cys = cysteine residues.

Seminal work in preparing models of  $[\text{NiFe}]$  hydrogenase mostly involved structural models, so as to obtain a better understanding of the structural properties of hydrogenases.<sup>10,11</sup> More recently, however, functional models capable of evolving dihydrogen have emerged. A very recent example of such a model complex, which closely resembles the core of  $[\text{NiFe}]$  hydrogenase, is the complex  $[\text{Ni}^{\text{II}}(\text{X}')\text{Fe}^{\text{II}}(\text{MeCN})\{\text{P-}$

**Received:** April 10, 2014

$(\text{OEt})_3\}_3][(\text{BPh}_4)_2]$  ( $X' = N,N'$ -diethyl-3,7-diazanonane-1,9-dithiolato) (Chart 2a) reported by Ogo and co-workers.<sup>12,13</sup>

**Chart 2. Molecular Structures of Recent Functional [NiFe] Hydrogenase Models:** (a)  $[\text{Ni}(X')\text{Fe}(\text{MeCN})\{\text{P}(\text{OEt})_3\}_3]^{2+}$ ; (b)  $[(\text{CO})_3\text{Fe}(\text{pdt})\text{NiH}(\text{dppe})]^+$



This system heterolytically activates dihydrogen at room temperature in the presence of sodium methoxide, and a proton is captured by the strong base and eliminated as methanol. Another such example is the complex  $[(\text{CO})_3\text{Fe}(\text{pdt})\text{NiH}(\text{dppe})]^+$  (Chart 2b) reported by Rauchfuss and co-workers in 2009.<sup>14</sup> The hydride form of this complex, at various molar equivalents of  $\text{CF}_3\text{COOH}$ , can evolve  $\text{H}_2$ , detected with cyclic voltammetry. A common feature of all existing functional mimics is the formation of a metal hydride as an intermediate.

The  $\text{Ni}(\mu\text{-S}_2)\text{Fe}$  core therefore plays a crucial role in biomimetic studies of [NiFe] hydrogenase, and synthetic access to and fundamental studies of this core in terms of its electrochemical behavior and reactivity is of fundamental importance. Herein we report a novel synthetic route to a  $\text{Ni}(\mu\text{-S}_2)\text{Fe}$  core, reminiscent of the core structure of the active site in [NiFe] hydrogenase, via a facile phosphine elimination approach. With the supersulfido nickel(II) complex **1** and the easily accessible zerovalent iron precursor  $\text{Fe}(\text{dmpe})_2(\text{PMe}_3)$  (**2**;  $\text{dmpe} = 1,2$ -bis(dimethylphosphino)ethane) as starting materials, the complex  $[(\text{Nacnac})\text{Ni}(\mu\text{-S}_2)\text{Fe}(\text{dmpe})_2]$  (**3**), bearing a monoradical  $\text{Ni}(\mu\text{-S}_2)\text{Fe}$  core and an  $\text{S}_2$  moiety of high “sub sulfide” ( $\text{S}_2^{3-}$ ) character can be isolated. Moreover, its reactivity, striking electrochemical properties, and full spectroscopic and structural elucidation as well as a detailed DFT study are reported here.

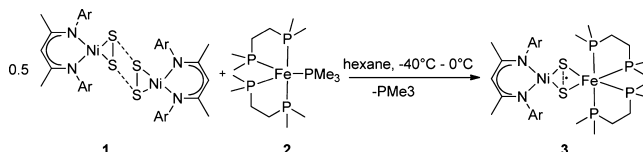
## RESULTS AND DISCUSSION

The starting point in our study is the supersulfido nickel(II) complex  $[(\text{Nacnac})\text{Ni}(\text{S}_2)]$  (**1**;  $\text{Nacnac} = \text{CH}\{(\text{CMe})-(2,6\text{-}^i\text{Pr}_2\text{C}_6\text{H}_3\text{N})\}_2$ ), reported by us recently.<sup>15</sup> Complex **1** is one of the few examples of a complex featuring a superhalogenide  $\text{S}_2^-$  ligand, easily accessible from the  $[(\text{Nacnac})\text{Ni}]_2(\mu\text{-toluene})$  complex upon reaction with elemental sulfur. The complex exists in the solid state as a diamagnetic dimer which dissociates in solution at room temperature to give the paramagnetic monomer  $[(\text{Nacnac})\text{NiS}_2]$ .<sup>15</sup> We reasoned that complex **1** represents an ideal reaction partner, which when reacted with a suitable iron precursor should form the  $\text{Ni}(\mu\text{-S}_2)\text{Fe}$  core, reminiscent of what is seen in the active site of [NiFe] hydrogenase. For this purpose,  $[(\text{dmpe})_2(\text{PMe}_3)\text{Fe}]$  (**2**;  $\text{dmpe} = 1,2$ -bis(dimethylphosphino)ethane)<sup>16</sup> represents an ideal iron(0) source, since it was previously shown to undergo facile  $\text{PMe}_3$  elimination, affording entry to complexes of the type  $[(\text{dmpe})_2\text{FeL}]$  ( $L = \sigma$ -donor,  $\pi$ -acceptor substituents).<sup>16a,17</sup>

In fact, the desired monoradical complex  $[(\text{Nacnac})\text{Ni}(\mu\text{-S}_2)\text{Fe}(\text{dmpe})_2]$  (**3**) is readily formed in a reaction of **1** with 1 molar equiv of **2** in hexane at  $-30^\circ\text{C}$ . A color change of the

solution from dark brown to light green indicated the completion of the reaction, and an in situ  $^{31}\text{P}\{^1\text{H}\}$  NMR spectrum of the resulting solution showed that  $\text{PMe}_3$  had been liberated. Workup afforded the novel complex **3** as a green solid in a yield of 75% as an extremely air and moisture sensitive compound (Scheme 1). In the solid state, compound **3** can be

**Scheme 1. Formation of the Complex 3 via Phosphine Elimination from the Iron(0) Precursor 2**



stored under inert conditions for several months, while in solutions at room temperature, it decomposes over a period of approximately 10 days to  $[(\text{Nacnac})\text{Ni}(\mu\text{-S}_2)\text{Ni}(\text{Nacnac})]$  (**8**)<sup>15</sup> and other intractable products.

Compound **3** was fully analyzed by a suite of spectroscopic and structural methods. The composition was additionally confirmed by HR-ESI-MS in THF. Crystals suitable for single-crystal X-ray diffraction analysis were obtained from recrystallization of **3** in a diethyl ether solution at ambient temperature. The molecular structure of the novel heterodinuclear [NiFe] compound **3** is shown in Figure 1 with some key metrical parameters. It crystallizes in the monoclinic space group  $P2_1/n$ . The nickel center is surrounded by two nitrogen atoms of the  $\beta$ -diketiminato ligand and two bridging sulfur atoms ( $\text{NiN}_2\text{S}_2$ ) in a roughly square planar coordination arrangement expected for a  $\text{Ni}^{\text{II}}$  site (see below). The iron center is octahedrally

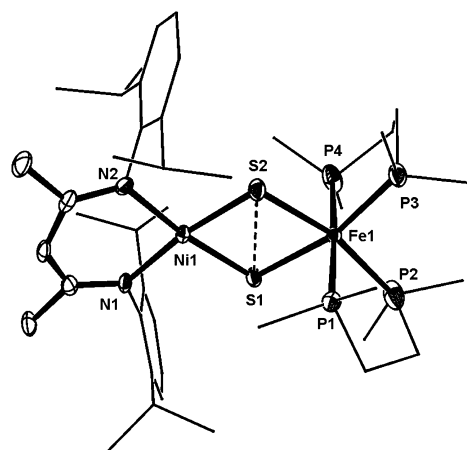


**Figure 1.** Molecular crystal structure of **3**. Thermal ellipsoids are drawn at the 50% probability level. Hydrogen atoms are omitted for clarity. Selected distances (Å) and angles (deg):  $\text{S1}\cdots\text{S2}$  2.742(2),  $\text{Ni1}\text{--}\text{Fe1}$  3.482(9),  $\text{Ni1}\text{--}\text{N2}$  1.962(4),  $\text{Ni1}\text{--}\text{N1}$  1.975(4),  $\text{Ni1}\text{--}\text{S1}$  2.128(2),  $\text{Ni1}\text{--}\text{S2}$  2.197(2),  $\text{Fe1}\text{--}\text{P3}$  2.200(2),  $\text{Fe1}\text{--}\text{P4}$  2.220(2),  $\text{Fe1}\text{--}\text{S1}$  2.225(2),  $\text{Fe1}\text{--}\text{P2}$  2.246(2),  $\text{Fe1}\text{--}\text{P1}$  2.246(2),  $\text{Fe1}\text{--}\text{S2}$  2.324(1);  $\text{N2}\text{--}\text{Ni1}\text{--}\text{N1}$  93.8(2),  $\text{N2}\text{--}\text{Ni1}\text{--}\text{S1}$  171.4(1),  $\text{N1}\text{--}\text{Ni1}\text{--}\text{S1}$  94.1(1),  $\text{N2}\text{--}\text{Ni1}\text{--}\text{S2}$  93.5(1),  $\text{N1}\text{--}\text{Ni1}\text{--}\text{S2}$  172.6(1),  $\text{S1}\text{--}\text{Ni1}\text{--}\text{S2}$  78.7(5),  $\text{P3}\text{--}\text{Fe1}\text{--}\text{P4}$  88.0(7),  $\text{P3}\text{--}\text{Fe1}\text{--}\text{S1}$  92.1(6),  $\text{P4}\text{--}\text{Fe1}\text{--}\text{S1}$  91.2(7),  $\text{P3}\text{--}\text{Fe1}\text{--}\text{P2}$  101.0(7),  $\text{P4}\text{--}\text{Fe1}\text{--}\text{P2}$  93.1(8),  $\text{S1}\text{--}\text{Fe1}\text{--}\text{P2}$  166.4(7),  $\text{P3}\text{--}\text{Fe1}\text{--}\text{P1}$  96.5(7),  $\text{P4}\text{--}\text{Fe1}\text{--}\text{P1}$  175.5(7),  $\text{S1}\text{--}\text{Fe1}\text{--}\text{P1}$  89.2(6),  $\text{P2}\text{--}\text{Fe1}\text{--}\text{P1}$  85.5(8),  $\text{P3}\text{--}\text{Fe1}\text{--}\text{S2}$  165.3(6),  $\text{P4}\text{--}\text{Fe1}\text{--}\text{S2}$  87.4(6),  $\text{S1}\text{--}\text{Fe1}\text{--}\text{S2}$  74.1(5),  $\text{P2}\text{--}\text{Fe1}\text{--}\text{S2}$  93.2(6),  $\text{P1}\text{--}\text{Fe1}\text{--}\text{S2}$  88.4(6),  $\text{Ni1}\text{--}\text{S1}\text{--}\text{Fe1}$  106.2(6),  $\text{Ni1}\text{--}\text{S2}\text{--}\text{Fe1}$  100.7(6).

coordinated by the four phosphorus atoms of two chelating dmpe ligands and two sulfur atoms bridging to the nickel center ( $\text{FeP}_4\text{S}_2$ ). The Ni–Fe distance of 3.482(9) Å suggests the absence of a Ni–Fe bond.<sup>18</sup> The metal centers are bridged by a disulfur subunit, forming the  $\text{Ni}(\mu\text{-S})_2\text{Fe}$  core similar to that of [NiFe] hydrogenase. The S1–S2 distance of 2.742(2) Å is similar to that in the previously reported and related complex [(Nanac)Ni( $\mu\text{-S}_2$ )Pt(PPh<sub>3</sub>)<sub>2</sub>] (7; 2.71 Å), suggesting the presence of an unpaired electron and significant  $\text{S}_2^{3-}$  subsulfide character (see below).<sup>19</sup> The Ni–S distances in 3 (Ni1–S1 2.128(2) Å and Ni1–S2 2.197(2) Å) are close to those of the starting complex 1 (2.163(1) and 2.166(1) Å).<sup>15</sup> The Fe–S distances (Fe1–S1 2.225(1) Å and Fe1–S2 2.324(1) Å) are comparable with Rauchfuss' [NiFe] hydrogenase model complex [(CO)<sub>3</sub>Fe(pdt)Ni(dppe)] (2.2835(9) and 2.2753(8) Å)<sup>20</sup> and close to those of the active site of *D. vulgaris Miyazaki* in the reduced form (2.29 and 2.36 Å).<sup>21</sup> The  $\text{Ni}(\mu\text{-S}_2)\text{Fe}$  core exhibits a V-shaped conformation with angles of 74.1(5)° (S1Ni1S2) and 78.7(5)° (S1Fe1S2). The latter value is close to the angle observed in the oxidized form of *D. gigas* (79.4°). Coordination of the  $\text{S}_2$  unit to the metal centers is somewhat asymmetric (Figure 1). This asymmetry and the slight twisting of the  $\text{S}_2$  unit out of the N1–Ni–N2 plane deviates somewhat from the genuine square-planar geometry expected for a low-spin Ni(II) center (see below).

The <sup>1</sup>H NMR spectrum of 3 in C<sub>6</sub>D<sub>6</sub> exhibits resonances paramagnetically shifted to high field ( $\delta$  –1.5, –1.7, –2.4, –3.2, and –10 ppm), most of which are substantially broadened. The <sup>31</sup>P{<sup>1</sup>H} NMR spectrum revealed no signals, consistent with the expectations for a paramagnetic complex. The assignment of the signals in the <sup>1</sup>H NMR spectrum was successfully accomplished by DFT calculations (see DFT Calculations for 3 and Related Complexes and the Supporting Information), which provided <sup>1</sup>H shifts in good agreement with experiment.

The paramagnetic nature of complex 3 prompted us to investigate its magnetic properties by superconducting quantum interference device (SQUID) measurements. The effective magnetic moment in the solid state was  $\mu_{\text{eff}} = 1.69 \mu_{\text{B}}$ , (in the range 2–310 K), indicative of a single electron located in the highest occupied molecular orbital HOMO of 3, in accordance with our structural studies.

Moreover, continuous wave X-band EPR spectroscopy of 3 (30 K) showed three different *g* values with  $g_1 \neq g_2 \neq g_3$  (2.200, 2.131, and 2.074, respectively). This is typical for the presence of an unpaired electron on atoms with a more than half-filled valence shell (i.e., sulfur or nickel; cf. Figure 2). The average *g* value ( $g_{\text{av}} = 2.136$ ) is much larger than the spin-only *g* value of 2.0023. The *g* values were also determined more accurately from a Q-band ESE detected EPR spectrum (Figure 2, top right), which features a higher resolution. As has been shown by calculations for the related [(Nanac)Ni( $\mu\text{-S}_2$ )Pt(PPh<sub>3</sub>)<sub>2</sub>] (7; see below),<sup>19</sup> the *g* tensor is dominated by spin–orbit contributions from the Ni atom, consistent with significant spin density on Ni. Further detailed EPR investigations of 3 with ENDOR (Figure 2, bottom left), ESEEM (Figure 2, bottom right), and HYSCORE techniques (see the Supporting Information) indicate that only weak hyperfine couplings with <sup>1</sup>H, <sup>31</sup>P, and <sup>15</sup>N nuclei are present. The combination of large positively shifted *g* values and small ligand hyperfine interactions indicates that the unpaired electron must be localized on the  $\text{Ni}(\mu\text{-S}_2)$  subunit of the core (see below). Moreover, since only weak coupling from the unpaired electron to <sup>1</sup>H was observed in the Davies ENDOR measurement at 10

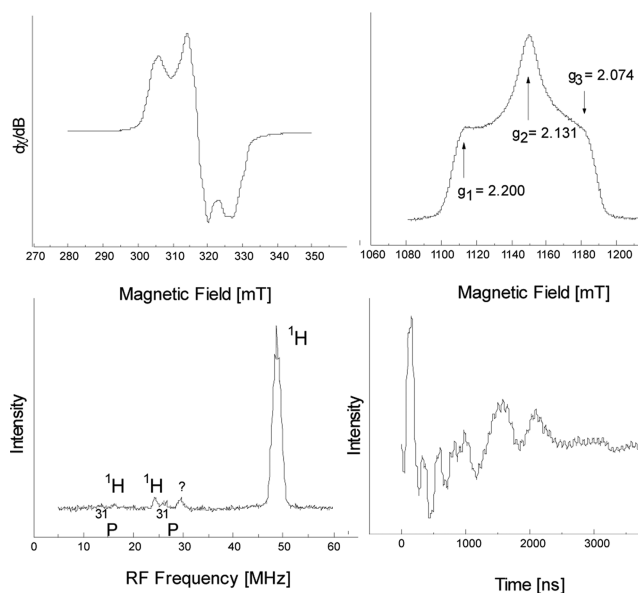


**Figure 2.** EPR measurements of compound 3: (top left) continuous wave X-band, with  $g_1 = 2.200$ ,  $g_2 = 2.131$ ,  $g_3 = 2.073$  (30 K, microwave frequency 9.476 GHz, power 2 mW, modulation amplitude 0.5 mT); (top right) ESE (electron spin echo) detected EPR spectrum ( $T = 10$  K, microwave frequency 34.288 GHz); (bottom left) Davies ENDOR (10 K, microwave frequency 34.288 GHz); (bottom right) ESEEM (10 K, microwave frequency 9.73 GHz, modulation amplitude 316.3 mT).

K, the ENDOR spectrum indicates that neither of the sulfur atoms of the  $\text{S}_2$  subunit can be protonated. Moreover, the ESEEM experiment clearly establishes rather strong echo modulations of nitrogen, also observed in the two-dimensional (HYSCORE) spectrum. This confirms delocalization of spin density from the  $\text{S}_2$  moiety over the Ni center. In addition, weak coupling to phosphorus is clearly observed in the Davies ENDOR spectrum.<sup>22</sup>

Compound 3 was also investigated by <sup>57</sup>Fe Mössbauer spectroscopy at 80 K to elucidate the formal oxidation state of the iron center (Figure 3). The zero-field <sup>57</sup>Fe Mössbauer spectrum of 3 at 80 K displays a quadrupole doublet, with the isomer shift  $\delta_{\text{is}} = 0.20 \text{ mm s}^{-1}$ , which falls in the typical range of octahedral  $d^6 \text{ Fe}^{\text{II}}$  low-spin phosphane complexes.<sup>23</sup> The isomer

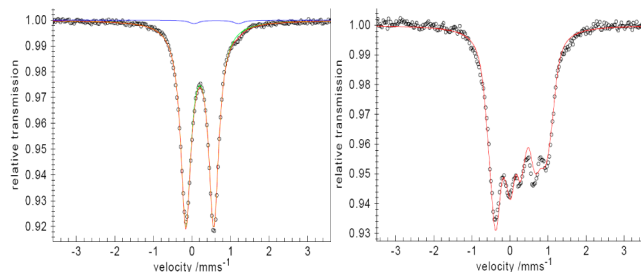


**Figure 3.** Zero-field <sup>57</sup>Fe Mössbauer spectrum of 3 at 80 K (left) and applied field <sup>57</sup>Fe Mössbauer measurement with 4.0 T at 4.2 K (right). The red line in the zero-field spectrum is the result of a fit with Lorentzian doublets, whereas for the magnetic spectrum the line results from a spin-Hamiltonian simulation for  $S = 1/2$  with *g* values .07, 2.21, and 2.13 taken from EPR and hyperfine parameters  $\delta = 0.21 \text{ mm s}^{-1}$ ,  $\Delta E_{\text{Q}} = 0.73 \text{ mm s}^{-1}$ ,  $\eta = 0.5$ , and  $A/g_N\mu_N = +2.29, -20.75, -16.37 \text{ T}$ , whereby *g*- and *A*-tensor components are given in the principal axis system of the EFG.

shift is comparable to the parameter of the Fe<sup>II</sup> low-spin complex [Fe(S<sub>2</sub>CH)(dmpe)<sub>2</sub>][BPh<sub>4</sub>] (0.17 mm s<sup>-1</sup>)<sup>23</sup> and is slightly larger than the shift range measured for [NiFe] hydrogenase (0.05–0.15 mm s<sup>-1</sup>).<sup>24</sup>

The electric quadrupole splitting of **3** is  $\Delta E_Q = 0.73$  mm s<sup>-1</sup>. This is comparable to that of the dithioformate iron complex [Fe(S<sub>2</sub>CH)(dmpe)<sub>2</sub>][BPh<sub>4</sub>], which exhibits a slightly smaller value of  $\Delta E_Q = 0.62$  mm s<sup>-1</sup>. Moreover, the applied field Mössbauer spectrum was also recorded at 4.0 T and 4.2 K. The combined effect of nuclear Zeeman, magnetic, and electric hyperfine coupling of **3** showed a characteristic magnetic splitting pattern of five peaks, which could be readily simulated with EPR *g* values and an anisotropic magnetic hyperfine coupling tensor of significant size:  $A/g_N\mu_N = +2.29, -20.75, -16.37$  T. The relatively large isotropic part,  $A_{\text{iso}}/g_N\mu_N = -11.6$  T, is confirmed by the DFT calculations (see below) and reflects some spin density on the iron center. Furthermore, the simulation reveals a negative sign of the main component of the electric field gradient (EFG) with moderately small asymmetry parameter ( $\eta = 0.5$ ).

#### DFT Calculations for **3** and Related Complexes.

Structural optimization of **3** at the PBE0(D3-BJ)/basis-1 level (see Computational Details) affords results which are in agreement with the X-ray diffraction data ( $d(\text{S}–\text{S}) = 2.749$  Å,  $d(\text{Ni}–\text{S}) = 2.232$  Å, 2.154 Å,  $d(\text{Fe}–\text{S}) = 2.305$  Å, 2.289 Å; see also Table S3 in the Supporting Information). The computed S–S distance is much larger than that expected for a disulfide ligand S<sub>2</sub><sup>2-</sup> and agrees well with those in the previously reported and related complexes [(Nacnac)Ni(μ-S<sub>2</sub>)Pt(PPh<sub>3</sub>)<sub>2</sub>] (**7**)<sup>19</sup> and [(tmeda)<sub>3</sub>Cu<sub>3</sub>S<sub>2</sub>]<sup>3+</sup>.<sup>25–27</sup> The last two complexes were studied previously in the context of the ongoing search for the elusive idealized “S<sub>2</sub><sup>3-</sup>” radical anion (see below).

Subsequent single-point DFT calculations of complex **3** (with basis-2) of paramagnetic NMR chemical shifts<sup>28</sup> and of the electronic *g* tensor also provide a good agreement with experiment, in particular when a modified B3LYP\*\* hybrid functional with 10% exact-exchange admixture is used (cf. Tables S4–S6 and Figure S5 in the Supporting Information). We had previously found similar performance for the related compound **7**.<sup>19</sup> This functional was thus used to examine, in detail, the spin-density distributions and electronic structure of **3** and of related oxidized and reduced compounds (using def2-TZVP basis sets). Moreover, the same functional was employed to compute the <sup>57</sup>Fe Mössbauer parameters (the nuclear quadrupole coupling, NQC, and the isomer shift,  $\delta_{\text{is}}$ ; see Computational Details). The calculated parameters compare reasonably well with experiment ( $\delta_{\text{is}}(\text{calcd}) = 0.36$  mm s<sup>-1</sup>,  $\delta_{\text{is}}(\text{exptl}) = 0.2$  mm s<sup>-1</sup>;  $\text{NQC}(\text{calcd}) = 0.77$  mm s<sup>-1</sup>,  $\text{NQC}(\text{exptl}) = 0.72$  mm s<sup>-1</sup>), although the computed asymmetry parameter ( $\eta = 0.36$ ) is somewhat lower than the experimental parameter. The <sup>57</sup>Fe hyperfine tensors were also computed (Table S7 in the Supporting Information) and are in excellent agreement with the experimental <sup>57</sup>Fe Mössbauer-derived data. This indicates that the hyperfine coupling is consistent with the non-negligible, but moderate, delocalization of spin density onto the iron center. Together with structure, NMR, and EPR data, the computed Mössbauer data thus provide good evidence for the correct description of the electronic structure at the given computational level, and the data agree well with the assignment to an octahedral low-spin Fe<sup>II</sup> state (see also below).

We had in previous studies demonstrated for **7** that, while the bridging S<sub>2</sub> ligand is rather close to an “S<sub>2</sub><sup>3-</sup>” state, partial

oxidation of the Ni center beyond the +2 oxidation state leads to a more reduced ligand, intermediate between S<sub>2</sub><sup>3-</sup> and two separated S<sup>2-</sup> ions. Consequently, the S–S bond order was found to be appreciably lower than the 0.5 expected for an idealized S<sub>2</sub><sup>3-</sup> ion. In **7**, the Pt center did not change its oxidation state beyond +2. Since the Fe<sup>II</sup> center in **3** is more likely to be oxidized, we applied the same extended set of electronic structure analyses to complex **3**, in addition to model complexes designed to provide more clear-cut S<sub>2</sub><sup>3-</sup> or S<sub>2</sub><sup>2-</sup> ligands. Table 1 provides computed atomic spin densities,

**Table 1.** NPA Spin Densities in Selected Systems<sup>a</sup>

complex	NPA spin density for M(1)S(1)S(2)M(2)			
	S(1)	S(2)	M(1)	M(2)
[LNi(μ-S <sub>2</sub> )Fe(dmpe) <sub>2</sub> ] ( <b>3</b> )	0.333	0.043	0.449	0.178
[LNi(μ-S <sub>2</sub> )Pt(PPh <sub>3</sub> ) <sub>2</sub> ] ( <b>7</b> )	0.341	0.078	0.452	0.021
[LZn(μ-S <sub>2</sub> )Pt(PPh <sub>3</sub> ) <sub>2</sub> ]	0.512	0.418	0.001	0.008
Na <sub>3</sub> S <sub>2</sub>	0.524	0.524	-0.016 <sup>b</sup>	
[(tmeda) <sub>3</sub> Cu <sub>3</sub> S <sub>2</sub> ] <sup>3+</sup>	0.235	0.235	0.281 <sup>b</sup>	

<sup>a</sup>B3LYP\*\*/def2-TZVP//PBE0(D3-BJ)/basis-1 results (cf. Computational Details). Core atoms are marked in boldface. L denotes the CH{(CMe)(2,6-*i*-Pr<sub>2</sub>C<sub>6</sub>H<sub>3</sub>N)}<sub>2</sub> ligand. <sup>b</sup>Average values over all Na and Cu atoms, respectively.

which are particularly informative. The S<sub>2</sub> units of **3** and **7** exhibit very similar and in both cases notably asymmetrical spin-density distributions on the two sulfur atoms. We had previously noted for **7** that the asymmetry is due to the twisting of the S<sub>2</sub> unit out of the N<sub>2</sub>Ni plane, which is closely related to the partial oxidation of the Ni center beyond a planar low-spin d<sup>8</sup> Ni<sup>II</sup> state. For complex **7**, sulfur atom S1 was found to be positioned out of the N<sub>2</sub>Ni plane and thereby acquired a somewhat larger Ni–S covalency than atom S2 (cf. NPA charges in the Supporting Information, Table S9). This also holds for complex **3**, albeit to a lesser extent, as confirmed by the fact that the overall spin density on the S<sub>2</sub> ligand is clearly less than the one electron expected for an ideal S<sub>2</sub><sup>3-</sup> ion and is closer to that of [(tmeda)<sub>3</sub>Cu<sub>3</sub>S<sub>2</sub>]<sup>3+</sup>.<sup>25–27</sup> In contrast, spin densities close to 0.5 on each of the two sulfur atoms are found for the idealized model systems Na<sub>3</sub>S<sub>2</sub> and [(Nacnac)Zn(μ-S<sub>2</sub>)Pt(PPh<sub>3</sub>)<sub>2</sub>] (Table 1). We demonstrated earlier for **7** that the distortion is an electronic effect allowing partial charge transfer from Ni<sup>II</sup> to a putative S<sub>2</sub><sup>3-</sup> ligand, rather than being caused by any steric restrictions. It is noteworthy that the Mayer bond order (MBO) computed for **3** is even slightly less than that for **7** (Table 2 below), significantly below the values obtained for systems with a more idealized “half-bond” between the two sulfur atoms.

Regarding the electronic situation at the iron center of **3**, we note that first its computed spin density is significantly larger than those on platinum in the two related complexes **7** and [(Nacnac)Zn(μ-S<sub>2</sub>)Pt(PPh<sub>3</sub>)<sub>2</sub>] (Figure 4; see also Figure S9 in the Supporting Information) but second it is much less than one would expect for a genuine Fe<sup>III</sup> complex. That is, the relatively low spin density on iron is not in contradiction with a predominant low-spin d<sup>6</sup> Fe<sup>II</sup> state inferred from the <sup>57</sup>Fe Mössbauer data. The spin density on Ni in **3** is very similar to that of **7**, indicating the same partial oxidation beyond Ni<sup>II</sup>.<sup>19</sup>

It is moreover instructive to examine how the molecular and electronic structure of **3** changes upon adding or removing one electron. Table 2 thus compares the corresponding S–S distances and computed NPA charges for the cation **4** and the

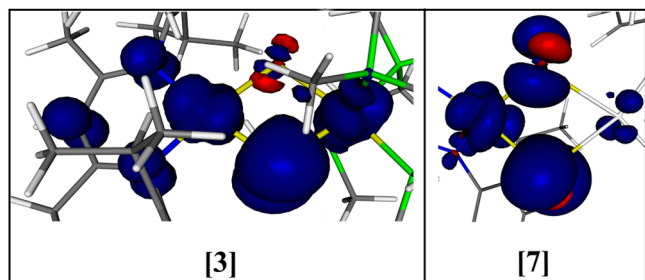


**Figure 4.** Spin-density distribution of **3** and **7** ( $\pm 0.002$  au isosurfaces). Positive spin density is indicated in blue and negative spin density in red.

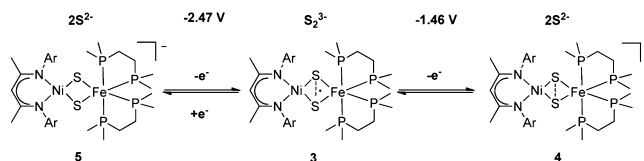
anion  $[(\text{Nacnac})\text{Ni}(\mu\text{-S})_2\text{Fe}(\text{dmpe})_2]^-$  (**5**) to those of neutral **3** and to a number of other model complexes. One-electron reduction of **3** affords an elongation of the S–S distance and increased negative charge on the bridging ligand, consistent with further reduction of this unit to two bridging  $\text{S}^{2-}$  ligands. Changes in the metal charges are minor, consistent with a ligand-centered reduction. This holds also for other model complexes examined for comparison (Table 2).

In the case of **7** and of other model complexes, we previously found that, upon oxidation of the monocation, the electron had also been removed predominantly from the  $\text{S}_2$  subunit, turning the ligand into the disulfide  $\text{S}_2^{2-}$  (with a much shorter, genuine S–S single bond). In the present case, cation **4** exhibits notable differences (Table 2): first of all, the S–S distance increases slightly rather than being reduced. Consequently, the MBO is further lowered, rather than increased. The main electronic change pertains to the NPA charge on iron, which is lowered by about one electron (whereas the charge on Ni changes only slightly). That is, the first oxidation of **3** is predicted to be metal-centered rather than ligand-centered, in contrast to the case for **7** or related complexes. This marks a notable difference, due to the presence of a redox-active second metal center. In fact, in comparison to **3**, in **4** the bridging unit has moved more into the direction of two  $\text{S}^{2-}$  ions rather than toward an  $\text{S}_2^{2-}$  ligand.

**Electrochemistry for Compound 3.** The redox behavior of complex **3** was also investigated with cyclic voltammetry.

The cyclic voltammogram revealed a quasi-reversible redox process at  $E_{1/2} = -2.47$  V vs  $\text{Fc}/\text{Fc}^+$  followed by an irreversible peak at  $E = -1.46$  V vs  $\text{Fc}/\text{Fc}^+$ . The one-electron reduction of **3** at  $-2.47$  V vs  $\text{Fc}/\text{Fc}^+$  may lead to the formation of an anionic species with two  $\text{S}^{2-}$ , while the one-electron oxidation of the monoradical **3** at  $-1.46$  V may furnish the cationic complex **4**. The various redox states of **3**, deduced from cyclic voltammetry, are shown in Scheme 2. In contrast to the

### Scheme 2. Proposed Structures of the Electrochemically Generated Oxidized (**4**) and Reduced (**5**) Species of (**3**)<sup>a</sup>



<sup>a</sup>See the Supporting Information, Figure S4.

$[(\text{Nacnac})\text{Ni}(\mu\text{-S}_2)\text{Pt}(\text{PPh}_3)_2]^{19}$  complex, the oxidation of the monoradical **3** seems to be irreversible. In the case of **3**, it appears from these data that the iron core is involved in the redox processes of the monoradical, in contrast to the case for the platinum core in  $[(\text{Nacnac})\text{Ni}(\mu\text{-S}_2)\text{Pt}(\text{PPh}_3)_2]$ . The compound  $[(\text{CO})_3\text{Fe}(\text{pdt})\text{Ni}(\text{dppe})]$  by Rauchfuss et al. shows oxidation to the monocationic species at  $E_{1/2} = -0.520$  V vs  $\text{Fc}/\text{Fc}^+$ . The comparison shows that the oxidation of **3** in cyclic voltammetry proceeds significantly more readily than for the Rauchfuss compound, as can be expected from the occupation of the HOMO with an unpaired electron.

**Reactivity of Complex 3.** Complex **3** is soluble in hydrocarbon solvents and decomposes slowly in ethereal solvents. It is very sensitive toward oxygen and moisture. The reactivity of complex **3** toward dihydrogen was also examined by treating a solution of **3** with 1 atm of dry dihydrogen at ambient temperature; however, no significant activation of dihydrogen was observed and the reaction only afforded decomposed products of **3**. However, inspired by the results of cyclic voltammetry, we became interested in exploring the redox behavior of **3** via synthetic methods, so as to perhaps obtain isolable reductive or oxidative products of **3**, which could

**Table 2.** Optimized S...S Distances (in Å), NPA Charges, and S...S Mayer Bond Orders (MBO) in Relevant Complexes<sup>a</sup>

system	$d(\text{S}-\text{S})$	$q(\text{S})^b$	$q(\text{M})$	$q(\text{M}')$	MBO
Neutral Complexes					
<b>3</b>	2.749	-0.167	0.293	-2.217	0.154
$[\text{LNi}(\mu\text{-S}_2)\text{Pt}(\text{PPh}_3)_2]$ ( <b>7</b> )	2.717	-0.493	0.873	0.131	0.215
$[\text{LZn}(\mu\text{-S}_2)\text{Pt}(\text{PPh}_3)_2]$	2.895	-0.734	1.553	0.146	0.330
$\text{Na}_3\text{S}_2$	3.421	-1.269	0.848 <sup>c</sup>		0.430
Oxidized Complexes					
<b>4</b>	2.780	-0.148	0.274	-1.081	0.108
$[\text{LNi}(\mu\text{-S}_2)\text{Pt}(\text{PPh}_3)_2]^+$	2.065	-0.178	0.781	0.104	0.947
$[\text{LZn}(\mu\text{-S}_2)\text{Pt}(\text{PPh}_3)_2]^+$	2.141	-0.398	1.564	0.112	0.942
$[\text{Na}_3\text{S}_2]^+$	2.226	-0.931	0.954 <sup>c</sup>		0.894
Reduced Complexes					
<b>5</b>	2.943	-0.763	0.246	-2.234	0.047
$[\text{LZn}(\mu\text{-S}_2)\text{Pt}(\text{PPh}_3)_2]^-$	3.278	-1.031	1.511	0.159	0.052
$[\text{Na}_3\text{S}_2]^-$	4.102	-1.533	0.689 <sup>c</sup>		0.042

<sup>a</sup>B3LYP\*\*/def2-TZVP//PBE0(D3-BJ)/basis-1 results (cf. Computational Details). Core atoms are marked in boldface. L denotes the  $\text{CH}\{\text{CMe}\}(2,6\text{-iPr}_2\text{C}_6\text{H}_3\text{N})_2$  ligand. <sup>b</sup>Average values over two S atoms. <sup>c</sup>Average value over all Na and Cu atoms, respectively (cf. Supporting Information for more details).

also be studied further. The oxidation of the monoradical **3** can be accomplished in a straightforward manner by the reaction with  $[(\eta^5\text{-C}_5\text{H}_5)_2\text{Fe}][\text{B}(\text{C}_6\text{H}_3(\text{CF}_3)_2)_4]$  in diethyl ether to afford the cationic complex  $[(\text{Nacnac})\text{Ni}(\mu\text{-S})_2\text{Fe}(\text{dmpe})_2]^+$  (**4**) in a yield of 51%. In contrast to complex **3**, **4** is a diamagnetic compound and has been characterized by mass spectrometry and NMR. Unfortunately, several attempts to obtain crystals of **4** suitable for X-ray diffraction analysis were unsuccessful. The DFT-optimized structure of cation **4**, including some key metrical parameters, is shown in Figure 5.

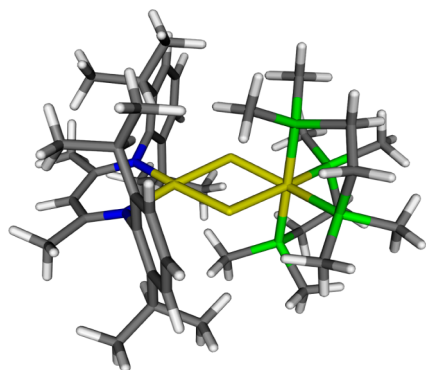


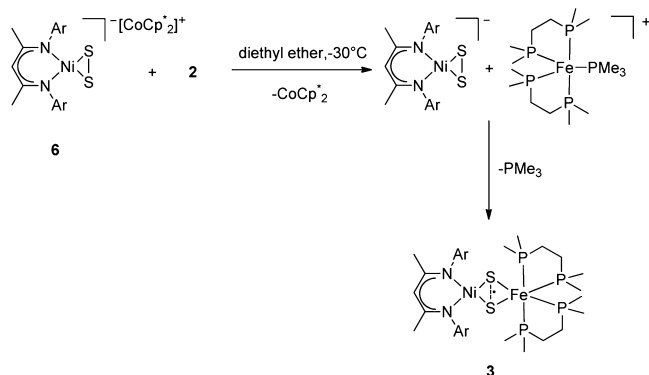
**Figure 5.** DFT-optimized structure of cation **4** (see the Supporting Information for more details). The Fe–Ni distance of 3.428 Å is somewhat shorter than that in the parent radical complex **3**: 3.546 Å (calculated), 3.482(9) Å (X-ray, vide supra).

The optimized structure shows a slight reduction in the Fe–Ni distance from 3.546 Å (calculated) to 3.428 Å vs 3.482(9) Å (X-ray, vide supra) in the parent radical complex **3**. The distance is still too large for an attractive Fe–Ni interaction.

The reduction of complex **3** was more complicated. In a number of reduction experiments, with different reducing agents ( $\text{KC}_8$ , K, Na naphthalenide), we generally obtained intractable reaction mixtures, and no products could be isolated. Hence, we decided to use  $[\text{Co}(\eta^5\text{-C}_5\text{Me}_5)_2][(\text{Nacnac})\text{NiS}_2]$  (**6**),<sup>29,30</sup> the reduced form of compound **1**. We expected that the reaction of **6** with Fe precursor **2** could, by a  $\text{PMe}_3$  elimination reaction similar to that described above, yield the desired  $[(\text{Nacnac})\text{Ni}(\mu\text{-S})_2\text{Fe}(\text{dmpe})_2]^-[\text{CoCp}^*]_2^+$  (**5**).

On the basis of spectroscopic analyses, reaction of **6** with **2** affords, as final products after workup, a mixture of radical complex **3** and neutral cobaltocene (Scheme 3). In order to

### Scheme 3. Proposed Mechanism of the Synthesis of **3** by the Reaction of the Anionic Complex **6** with **2**



shed light on this observation, we examined the electrochemical potential of **2** and decamethylcobaltocene in THF under the same conditions by cyclic voltammetry.<sup>16b</sup> According to this, the potential of **2** is more negative than that of decamethylcobaltocene. The latter implies that the decamethylcobaltocenium cation in **6** may be reduced before the combination of the nickel-containing disulfide anion with the iron complex. The coordination of the disulfide anion of **6** to the oxidized iron center and subsequently the reduction of the disulfide within the complex thus affords **3** as the final product.

## CONCLUSION

By employing the supersulfido nickel(II) complex  $[(\text{Nacnac})\text{Ni}(\text{S}_2)]$  (**1**) and the electron-rich iron(0) precursor  $[(\text{dmpe})_2(\text{PMe}_3)\text{Fe}]$  (**2**), the unusual monoradical  $[(\text{Nacnac})\text{Ni}(\mu\text{-S}_2)\text{Fe}(\text{dmpe})_2]$  complex **3** could be synthesized, with a core structure reminiscent of that in  $[\text{NiFe}]$  hydrogenase. Complex **3** was fully characterized structurally and spectroscopically, and in addition detailed DFT studies were carried out, elucidating the nature of the unique monoradical  $\text{Ni}(\mu\text{-S}_2)$  Fe core. Complex **3** bears a disulfur bridge with significant “subdisulfide”  $\text{S}_2^{3-}$  character. Alternatively, complex **3** can be accessed by a reductive route upon reaction of  $[\text{Co}(\eta^5\text{-C}_5\text{Me}_5)_2][(\text{Nacnac})\text{NiS}_2]$  (**6**) with **2**, affording complex **3** and “free”  $[\text{Co}(\eta^5\text{-C}_5\text{Me}_5)_2]$ . In addition, the oxidation reaction of **3** with  $[(\eta^5\text{-C}_5\text{H}_5)_2\text{Fe}][\text{B}(\text{C}_6\text{H}_3(\text{CF}_3)_2)_4]$  affords  $[(\text{Nacnac})\text{Ni}(\mu\text{-S})_2\text{Fe}(\text{dmpe})_2][\text{B}(\text{C}_6\text{H}_3(\text{CF}_3)_2)_4]$  (**4**). Although the activation of dihydrogen with complex **3** was not successful, the radical character of the disulfide bridge may pave the way to functionalize the sulfur bridge between the nickel and iron centers with suitable organic substrates. The synthetic methodology outlined here could hence enable entry to better structural or even functional models of  $[\text{NiFe}]$  hydrogenases, given the ease of access to the  $\text{Ni}(\mu\text{-S}_2)\text{Fe}$  core. Investigations in this direction are currently in progress.

## EXPERIMENTAL SECTION

**General Considerations.** All experiments and manipulations were carried out under dry oxygen-free nitrogen using standard Schlenk techniques or in an M. Braun inert-atmosphere drybox containing an atmosphere of purified nitrogen. Solvents were dried by standard methods and freshly distilled prior to use. The starting materials **1**,<sup>15</sup> **2**,<sup>16</sup> **6**,<sup>29</sup> and  $[(\eta^5\text{-C}_5\text{H}_5)_2\text{Fe}][\text{B}(\text{C}_6\text{H}_3(\text{CF}_3)_2)_4]$ <sup>31</sup> were prepared according to literature procedures. High-resolution ESI-MS were measured on a Thermo Scientific LTQ orbitrap XL instrument. <sup>1</sup>H and <sup>31</sup>P NMR spectra were recorded on Bruker APX 200 and AV 400 spectrometers, and chemical shifts are referenced to the <sup>1</sup>H NMR signal of tetramethylsilane (TMS) and the <sup>31</sup>P NMR signal of 85%  $\text{H}_3\text{PO}_4$ , respectively.

X-band EPR continuous wave EPR spectra were recorded on a Bruker ELEXSYS E500 spectrometer equipped with the Bruker standard cavity (ER4102ST) and a helium flow cryostat (Oxford Instruments ESR 910). Microwave frequencies were calibrated with a Hewlett-Packard frequency counter (HP352B), and the field control was calibrated with a Bruker NMR field probe (ER03SM). The spectra were simulated with the program GFIT (by E.B.) for the calculation of powder spectra with effective *g* values and anisotropic line widths (mixed Lorentzian and Gaussian line shapes were used). Pulsed EPR spectra were recorded on a Bruker SuperQ FT EPR spectrometer and a Bruker E580 spectrometer.

Mössbauer spectra were recorded on a conventional spectrometer with alternating constant acceleration of the  $\gamma$  source. The minimum experimental line width was 0.24  $\text{mm s}^{-1}$  (full width at half-height). The sample temperature was maintained constant in an Oxford Instruments Variox or Spectromag cryostat, with the field at the

sample being perpendicular to the  $\gamma$  beam. The  $^{57}\text{Co}/\text{Rh}$  source (1.8 GBq) was positioned at room temperature inside the gap of the spectromag system at a zero-field position, by using a re-entrant bore. Isomer shifts are quoted relative to iron metal at 300 K. Magnetic Mössbauer spectra were simulated with the program MX (by E.B.) by diagonalization of the spin Hamiltonian for  $S = 1/2$  and the usual nuclear Hamiltonian.<sup>65</sup>

Magnetic susceptibility data were measured from powder samples of solid material in the temperature range 2–300 K by using a SQUID susceptometer with a field of 1.0 T (MPMS-7, Quantum Design, calibrated with standard palladium reference sample, error <2%). The experimental data were corrected for underlying diamagnetism by use of tabulated Pascal's constants, as well as for temperature-independent paramagnetism. The susceptibility and magnetization data were simulated with our own package julX for exchange-coupled systems.

Infrared measurements in potassium bromide were recorded at room temperature on a Perkin-Elmer 100 FT-IR spectrometer. The spectrometer has an optical range of 7800–370  $\text{cm}^{-1}$  and a DTGS (deuterated triglycine sulfate) detector.

For single-crystal X-ray structure determinations, crystals were each mounted on a glass capillary in perfluorinated oil and measured in a cold  $\text{N}_2$  flow. The data of compound 3 was collected on an Oxford Diffraction Xcalibur S Sapphire at 150 K (Mo  $K\alpha$  radiation,  $\lambda = 0.71073 \text{ \AA}$ ). The structures were solved by direct methods and refined on  $F^2$  with the SHELX-97 software package.<sup>32</sup> The positions of the H atoms were calculated and considered isotropically according to a riding model. CCDC 958339 (3) contains supplementary crystallographic data for this paper. These data can be obtained free of charge by contacting The Cambridge Crystallographic Data Center, 12, Union Road, Cambridge CB2 1EZ, U.K.; fax +44 1223 336033.

**[(Nacnac)Ni( $\mu$ -S)<sub>2</sub>Fe(dmpe)<sub>2</sub>] (3).** The ( $\beta$ -diketiminato)nickel supersulfide 1 (200 mg, 0.185 mmol) and [(dmpe)<sub>2</sub>(PMe<sub>3</sub>)Fe] (2; 160.1 mg, 0.370 mmol) were dissolved in 30 mL of hexane. The solution was stirred for 30 min at  $-30 \text{ }^\circ\text{C}$ . The solution changed color to bottle green. The reaction mixture was filtered via filter cannula at low temperatures ( $0 \text{ }^\circ\text{C}$ ). The remaining dark brown residue was extracted with hexane ( $2 \times 10 \text{ mL}$ ). All filtrates were combined, and the volatiles were removed under reduced pressure to afford a dark green solid of 3 (249 mg, 0.277 mmol, 75%). For the single-crystal X-ray diffraction investigation, 3 was recrystallized in a small amount of diethyl ether at room temperature.  $^1\text{H}$  NMR (200.13 MHz,  $\text{C}_6\text{D}_6$ , 298 K):  $\delta$  8.72 (s,  $\Delta\nu_{1/2} = 18.4 \text{ Hz}$ , Ar-H, *m*-position); 7.94 (s,  $\Delta\nu_{1/2} = 18.2 \text{ Hz}$ , CHMe<sub>2</sub>); 7.41 (s,  $\Delta\nu_{1/2} = 38.2 \text{ Hz}$ , CHCH<sub>3</sub>CH<sub>3</sub>); 5.05 (s,  $\Delta\nu_{1/2} = 33.2 \text{ Hz}$ , Ar-H, *p*-position); 1.99 (br s,  $\Delta\nu_{1/2} = 15.4 \text{ Hz}$ , CHCH<sub>3</sub>CH<sub>3</sub>); 1.77 (br s,  $\Delta\nu_{1/2} = 21.2 \text{ Hz}$ , PCH<sub>3</sub>); 1.62 (s,  $\Delta\nu_{1/2} = 10.4 \text{ Hz}$ ); -1.57 (br s,  $\Delta\nu_{1/2} = 12.8 \text{ Hz}$ ); -1.77 (br s,  $\Delta\nu_{1/2} = 29.7 \text{ Hz}$ , PCH<sub>3</sub>); -2.42 (br s,  $\Delta\nu_{1/2} = 28.5 \text{ Hz}$ ); -3.20 (br s,  $\Delta\nu_{1/2} = 26.7 \text{ Hz}$ ); -10.16 (br s,  $\Delta\nu_{1/2} = 64.2 \text{ Hz}$  NCCH<sub>3</sub>), -39.05 (br s,  $\Delta\nu_{1/2} = 108.4 \text{ Hz}$   $\gamma$ -H) ppm. According to the broadening of the signals in the  $^1\text{H}$  NMR and the absence of resonance signals in  $^{31}\text{P}\{^1\text{H}\}$  and  $^{13}\text{C}\{^1\text{H}\}$  NMR, complex 3 is paramagnetic. HR APCI-MS (toluene):  $m/z$  calcd for (Nacnac)Ni( $\mu$ -S)<sub>2</sub>Fe(dmpe)<sub>2</sub> [ $\text{M}^+$ ] ( $\text{C}_{41}\text{H}_{73}\text{FeN}_2\text{NiP}_4\text{S}_2$ ) 895.2863, found 895.2857.  $^{57}\text{Fe}$  zero field Mössbauer (80 K):  $\delta = 0.20 \text{ mm s}^{-1}$ ;  $\Delta E_{\text{Q}} = 0.72 \text{ mm s}^{-1}$ , width =  $0.32 \text{ mm s}^{-1}$ ; depth =  $7.70 \text{ mm s}^{-1}$ . Applied field  $^{57}\text{Fe}$  Mössbauer measurement (4.0 T, 4.2 K):  $\delta = 0.21 \text{ mm s}^{-1}$ ,  $\Delta E_{\text{Q}} = 0.73 \text{ mm s}^{-1}$ , width =  $0.26 \text{ mm s}^{-1}$ . X-band EPR (9.476 GHz, 2 mW, 0.5 mT, 30 K):  $g_1 = 2.200$ ,  $g_2 = 2.131$ ,  $g_3 = 2.073$ . SQUID:  $\mu_{\text{eff}} = 1.69 \mu_{\text{B}}$ . IR (KBr,  $\text{cm}^{-1}$ ):  $\nu$  518 (w), 641 (m), 684 (m), 712 (m), 785 (m), 830 (m), 877 (s), 927 (s), 1022 (w), 1094 (w), 1110 (w), 1175 (m), 1251 (m), 1270 (m), 1316 (m), 1357 (m), 1407 (s), 1432 (s), 1464 (m), 1525 (s), 2864 (s), 2903 (s), 2925 (s), 2953 (s), 3052 (m).

**Alternative Synthesis of [(Nacnac)Ni( $\mu$ -S)<sub>2</sub>Fe(dmpe)<sub>2</sub>] (3).** The ( $\beta$ -diketiminato)nickel supersulfido anion 6 (100 mg, 0.115 mmol) and the complex [(dmpe)<sub>2</sub>(PMe<sub>3</sub>)Fe] (2; 50 mg, 0.115 mmol) were dissolved in diethyl ether at  $-30 \text{ }^\circ\text{C}$ . The reaction mixture was stirred for 1 h. The diethyl ether was removed under reduced pressure, and the residue was extracted with hexane and separated from small quantities of an insoluble solid via filter cannula. The hexane was removed in vacuo to afford a mixture of free cobaltocene and

compound 3 as a brown solid (65 mg). Both products were positively identified on the basis of NMR spectroscopy on comparison to authentic samples.

**[(Nacnac)Ni( $\mu$ -S)<sub>2</sub>Fe(dmpe)<sub>2</sub>][B(C<sub>6</sub>H<sub>3</sub>(CF<sub>3</sub>)<sub>2</sub>)<sub>4</sub>] (4).** In 30 mL of diethyl ether, complex 3 (150 mg, 0.167 mmol) and [ $\eta^5$ -C<sub>3</sub>H<sub>5</sub>)<sub>2</sub>Fe]-[B(C<sub>6</sub>H<sub>3</sub>(CF<sub>3</sub>)<sub>2</sub>)<sub>4</sub>] (190 mg, 0.184 mmol) were stirred at  $-30 \text{ }^\circ\text{C}$ . The color changed from grass green to a light green. After a reaction time of 30 min, the solution was filtered via cannula. The volatiles were removed under reduced pressure to afford 4 as a light green solid (150 mg, 0.084 mmol, 51%).  $^1\text{H}$  NMR (200.13 MHz,  $\text{CD}_2\text{Cl}_2$ , 298 K):  $\delta$  7.72 (s, 8H, B(C<sub>6</sub>H(CF<sub>3</sub>)<sub>2</sub>H<sub>2</sub>)<sub>4</sub>); 7.56 (s, 4H, B(C<sub>6</sub>H(CF<sub>3</sub>)<sub>2</sub>H<sub>2</sub>)<sub>4</sub>); 7.03 (s, 6H, Ar-H); 4.84 (s, 1H,  $\gamma$ -H); 4.26 (br s, 2H, PCH<sub>2</sub>); 4.02 (br s, 2H, PCH<sub>2</sub>); 2.34 (s, 2H, PCH<sub>2</sub>); 2.25 (br s, 4H, CH(CH<sub>3</sub>)<sub>2</sub>); 1.61 (s, 6H, NCCH<sub>3</sub>); 1.48 (br s, 24H, CH(CH<sub>3</sub>)<sub>2</sub>); 1.15 (pent, 24H, P(CH<sub>3</sub>)<sub>2</sub>); 1.08 (s, 2H, PCH<sub>2</sub>).  $^{31}\text{P}\{^1\text{H}\}$  NMR (81.01 MHz,  $\text{CD}_2\text{Cl}_2$ , 298 K):  $\delta = 38.8$  (s).  $^{11}\text{B}\{^1\text{H}\}$  NMR (64.21 MHz,  $\text{CD}_2\text{Cl}_2$ , 298 K):  $\delta = -6.6$  (s).  $^{19}\text{F}\{^1\text{H}\}$  NMR (188.31 MHz,  $\text{CD}_2\text{Cl}_2$ , 298 K):  $\delta = -62.3$  (s). HR ESI-MS (ion spray voltage 5 kV, flow rate 5  $\mu\text{L}/\text{min}$ , in THF):  $m/z$  calcd for [(Nacnac)Ni( $\mu$ -S)<sub>2</sub>Fe(dmpe)<sub>2</sub>]<sup>+</sup> [ $\text{M}^+$ ] ( $\text{C}_{41}\text{H}_{73}\text{FeN}_2\text{NiP}_4\text{S}_2$ ) 895.2863, found 895.2872. Negative HR ESI-MS:  $m/z$  calcd for [BArf]<sup>-</sup> [ $\text{M}^-$ ] ( $\text{C}_{32}\text{H}_{12}\text{BF}_4$ ) 863.0643, found 863.0625.

**Computational Details.** All structures were optimized in unrestricted (generalized) Kohn–Sham calculations with the Turbomole program package,<sup>33</sup> using the hybrid functional PBE0<sup>34–36</sup> augmented by Grimme's D3 dispersion corrections with Becke–Johnson damping<sup>37,38</sup> (PBE0(D3-BJ)). Standard Turbomole all-electron def2-TZVP basis sets<sup>39</sup> were used for Ni and Fe, together with smaller def2-SVP basis sets<sup>39</sup> for all other atoms (we will denote this combination “basis-1”). The crystal structure of 3 was used as the starting point for full optimization. Subsequent single-point calculations of magnetic resonance parameters (electronic  $\mathbf{g}$  tensor and  $^{57}\text{Fe}$  hyperfine tensors, NMR shifts) used modified (15s11p6d)/[9s7p4d] basis sets for Ni and Fe,<sup>40</sup> together with Huzinaga–Kutzelnigg-type IGLO-III basis sets<sup>41</sup> on the ligand atoms (basis-2). The resulting Kohn–Sham orbitals were transferred from Gaussian09<sup>42</sup> to the in-house program MAG-ReSpect,<sup>43</sup> which was used to carry out coupled-perturbed Kohn–Sham (CPKS) electronic  $\mathbf{g}$ -tensor and hyperfine calculations,<sup>44,45</sup> employing a common gauge origin at Ni for the  $\mathbf{g}$ -tensor calculation (cf. Table S4 in the Supporting Information). To assess the effect of exact Hartree–Fock (HF) exchange admixture, different exchange-correlation functionals have been tested: the BP86 “pure” functional,<sup>46–48</sup> the B3LYP hybrid functional with 20% exact-exchange admixture,<sup>49–51</sup> and the tailored B3LYP\*\* global hybrid with reduced admixture (10%). All spin–orbit (SO) matrix elements have been obtained within the accurate and efficient atomic mean-field approximation (AMFI)<sup>52,53</sup> to the full many-electron Breit–Pauli SO operator. Nuclear shieldings were computed with the same set of functionals and basis-2, using an in-house program,<sup>54</sup> which collects the necessary terms for open-shell shielding calculations and included all relevant terms for  $S = 1/2$  systems, which are often divided into an orbital term ( $\sigma_{\text{orb}}$ ) as well as temperature-dependent hyperfine-related contact and pseudocontact shifts.<sup>28</sup> For the latter, prior computation of EPR hyperfine couplings (HFCs) and the electronic  $\mathbf{g}$  tensor is needed. While the  $\mathbf{g}$  tensor was obtained as described above, the orbital term (in an open-shell generalization, using gauge-including atomic orbitals, GIAOs<sup>55</sup>) and the HFCs (neglecting SO contributions) were computed with Gaussian 09.<sup>42</sup> The hyperfine shifts were computed at 298 K. The calculated  $^1\text{H}$  shieldings were converted to chemical shifts ( $\delta$ , in ppm) relative to the shielding ( $\sigma(^1\text{H}) = 31.4$  ppm) of tetramethylsilane (TMS), obtained at the same computational level. The calculated NMR shifts of the alkyl and aryl groups were averaged between magnetically equivalent nuclei (assuming free rotation of CH<sub>3</sub> groups). Mössbauer parameters (nuclear quadrupole coupling tensors, NQC, and isomer shifts) were obtained with a large uncontracted def2-QZVP<sup>39</sup> basis at the iron atom together with a def2-TZVP<sup>39</sup> basis set for nickel and def2-SVP<sup>39</sup> basis sets for the ligand atoms (“basis-3”), using MAG-ReSpect. While the NQCs were directly computed as expectation values, a commonly used calibration was used to convert computed total densities at the nuclear position into isomer

shifts. We employed Neese's training set of 15 molecules.<sup>56–58</sup> The molecules of the training set, as well as the structure of **3**, were optimized at the PBE0(D3-BJ)/basis-1 level, followed by B3LYP\*\*/basis-3 single-point calculations. Atomic charges and spin densities were evaluated at the B3LYP\*\*/def2-TZVP//PBE0(D3-BJ)/basis-1 level by means of natural population analyses (NPA),<sup>59</sup> using the built-in NBO subroutines of the Gaussian 09 program.<sup>60</sup> The optimized structures of [LNiS<sub>2</sub>Pt(PPh<sub>3</sub>)<sub>2</sub>]<sup>1+/0</sup>, [LZnS<sub>2</sub>Pt(PPh<sub>3</sub>)<sub>2</sub>]<sup>1+/0/-</sup>, [Na<sub>3</sub>S<sub>2</sub>]<sup>+0/-</sup>, and [(tmeda)<sub>3</sub>Cu<sub>3</sub>S<sub>2</sub>]<sup>3+</sup> were taken from ref 19. Spin densities are provided either as isosurface plots ( $\pm 0.002$  au) or as NPA atomic values. Mayer bond orders<sup>61,62</sup> were evaluated at the same level, using the program BORDER.<sup>63</sup> The visualization of molecules, spin-density distributions, and orbitals was done with Molekel.<sup>64</sup>

## ■ ASSOCIATED CONTENT

### ● Supporting Information

Figures, tables, and a CIF file giving X-ray diffraction crystal data for **3**, SQUID, cyclic voltammetry, and HYSCORE EPR data, and theoretical calculations of **3**. This material is available free of charge via the Internet at <http://pubs.acs.org>.

## ■ AUTHOR INFORMATION

### Corresponding Authors

\*M.K.: e-mail, [martin.kaupp@tu-berlin.de](mailto:martin.kaupp@tu-berlin.de).

\*M.D.: e-mail, [matthias.driess@tu-berlin.de](mailto:matthias.driess@tu-berlin.de); web, <http://www.driess.tu-berlin.de>.

### Notes

The authors declare no competing financial interest.

## ■ ACKNOWLEDGMENTS

This work has been funded within the DFG excellence cluster *Unifying concepts in catalysis* (Unicat). F.M. is grateful for a scholarship from the Unicat within the framework of the Berlin graduate school of natural sciences and engineering (BIG-NSE). He thanks Dr. T. Pennanen for the implementation of Moessbauer parameter calculations into the local MAG/ReSpect program and S. Gasshemi Tabrizi and K. Theilacker for help with fitting the isomer shifts.

## ■ REFERENCES

- (1) Volbeda, A.; Fontecilla-Camps, J. C. *Top. Organomet. Chem.* **2006**, *17*, 57.
- (2) Russell, M. J.; Martin, W. *Trends Biochem. Sci.* **2004**, *29*, 358.
- (3) Covover, R. C.; Park, J.-B.; Adams, M. W. W.; Johnson, M. K. *J. Am. Chem. Soc.* **1990**, *112*, 4562.
- (4) (a) Ciurli, S.; Ross, P. K.; Scott, M. J.; Yu, S.-B.; Holm, R. H. *J. Am. Chem. Soc.* **1992**, *114*, 5415. (b) Panda, R.; Zhang, Y.; McLauchlan, C. C.; Venkateswara Rao, P.; Tiago de Oliveira, F. A.; Münck, E.; Holm, R. H. *J. Am. Chem. Soc.* **2004**, *126*, 6448.
- (c) Venkateswara Rao, P.; Holm, R. H. *Chem. Rev.* **2004**, *104*, 527.
- (5) Gloaguen, F.; Rauchfuss, T. B. *Chem. Soc. Rev.* **2009**, *38*, 100.
- (6) Lubitz, W.; Reijerse, E.; van Gestel, M. *Chem. Rev.* **2007**, *107*, 4331.
- (7) Ohki, Y.; Tatsumi, K. *Eur. J. Inorg. Chem.* **2011**, 973.
- (8) Darensbourg, M. Y.; Weigand, W. *Eur. J. Inorg. Chem.* **2011**, 994.
- (9) Volbeda, A.; Charon, M.-H.; Piras, C.; Hatchikian, E. C.; Frey, M.; Fontecilla-Camps, J. C. *Nature* **1995**, *373*, 580.
- (10) (a) Bouwman, E.; Reedijk, J. *Coord. Chem. Rev.* **2005**, *249*, 1555. (b) Heinekey, D. M. *J. Organomet. Chem.* **2009**, *694*, 2671.
- (11) Yamamura, Y.; Miyamae, H.; Katayama, Y.; Sasaki, Y. *Chem. Lett.* **1985**, 269.
- (12) Ogo, K. I.; Seiji, K.; Kishima, T.; Matsumoto, T.; Nakai, H.; Kusaka, K.; Ohhara, T. *Science* **2013**, *339*, 682.
- (13) Simmons, T. R.; Artero, V. *Angew. Chem., Int. Ed.* **2013**, *52*, 6143.
- (14) Barton, B. E.; Whaley, C. M.; Rauchfuss, T. B.; Gray, D. L. *J. Am. Chem. Soc.* **2009**, *131*, 6942.
- (15) Yao, S.; Milsman, C.; Bill, E.; Wieghardt, K.; Driess, M. *J. Am. Chem. Soc.* **2008**, *130*, 13536.
- (16) (a) Blom, B. *Reactivity of Ylenes at Late Transition Metal Centers*; Cuvilier Verlag: Göttingen and Bonn, Germany, 2011. (b) Electrochemical potentials: for **3**,  $E_{1/2} = -1.93$  V; for Co( $\eta^5$ -C<sub>5</sub>Me<sub>5</sub>)<sub>2</sub>,  $E_{1/2} = -1.75$  V; measured in THF at room temperature against Fc/Fc<sup>+</sup>; scan rate 100 mV/s; Biologic potentiostat SP-150; working electrode glassy carbon; counter electrode Pt; reference electrode Ag/Ag<sup>+</sup> pseudo reference; 0.3 M TBAPF<sub>6</sub>; EC-lab software V10.36.
- (17) Blom, B.; Enthaler, S.; Inoue, S.; Irran, E.; Driess, M. *J. Am. Chem. Soc.* **2013**, *135*, 6703.
- (18) Lindahl, P. A. *J. Inorg. Biochem.* **2012**, *106*, 172.
- (19) Yao, S.; Hrobárik, P.; Meier, F.; Rudolph, R.; Bill, E.; Irran, E.; Kaupp, M.; Driess, M. *Chem. Eur. J.* **2013**, *19*, 1246.
- (20) Zhu, W.; Marr, A. C.; Wang, Q.; Neese, F.; Spencer, D. J. E.; Blake, A. J.; Cooke, P. A.; Wilson, C.; Schröder, M. *Proc. Natl. Acad. Sci. U.S.A.* **2005**, *102*, 18280.
- (21) Higuchi, Y.; Ogata, H.; Miki, K.; Yasuoka, N.; Yagi, T. *Structure* **1999**, *7*, 549.
- (22) Bührke, T.; Brecht, M.; Lubitz, W.; Friedrich, B. *J. Biol. Inorg. Chem.* **2002**, *7*, 897.
- (23) Evans, D. J.; Jimenez-Tenorio, M.; Leigh, G. J. *J. Chem. Soc., Dalton Trans.* **1991**, 1785.
- (24) Surerus, K. K.; Chen, M.; van der Zwaan, J. W.; Rusnak, F. M.; Kolk, M.; Duin, E. C.; Albracht, S. P. J.; Muenck, E. *Biochemistry* **1994**, *33*, 4980.
- (25) Alvarez, S.; Hoffmann, R.; Mealli, C. *Chem. Eur. J.* **2009**, *15*, 8358.
- (26) Berry, J. F. *Chem. Eur. J.* **2010**, *16*, 2719.
- (27) Mealli, C.; Ienco, A.; Poduska, A.; Hoffmann, R. *Angew. Chem., Int. Ed.* **2008**, *47*, 2864.
- (28) Hrobárik, P.; Reviakine, R.; Arbuznikov, A. V.; Malkina, O. L.; Malkin, V. G.; Kohler, F. H.; Kaupp, M. *J. Chem. Phys.* **2007**, *126*, 024107.
- (29) Rudolph, R.; Yao, S.; Driess, M. Unpublished results.
- (30) Bai, G.; Wei, P.; Stephan, D. W. *Organometallics* **2005**, *24*, 5901.
- (31) Nafady, A.; Chin, T. T.; Geiger, W. E. *Organometallics* **2006**, *25*, 1654.
- (32) Sheldrick, G. M. *SHELX-97*; Universität Göttingen, Göttingen, Germany, 1997.
- (33) *TURBOMOLE v 6.3.1*; TURBOMOLE GmbH (since 2007), 1989–2007; available from <http://www.turbomole.com>.
- (34) Perdew, J. P.; Burke, K.; Ernzerhof, M. *Phys. Rev. Lett.* **1996**, *77*, 3865.
- (35) Perdew, J. P.; Burke, K.; Ernzerhof, M. *Phys. Rev. Lett.* **1997**, *78*, 1396.
- (36) Adamo, C.; Barone, V. *J. Chem. Phys.* **1999**, *110*, 6158.
- (37) Grimme, S.; Antony, J.; Ehrlich, S.; Krieg, H. *J. Chem. Phys.* **2010**, *132*, 154104.
- (38) Grimme, S.; Ehrlich, S.; Goerigk, L. *J. Comput. Chem.* **2011**, *32*, 1456.
- (39) Weigend, F.; Ahlrichs, R. *Phys. Chem. Chem. Phys.* **2005**, *7*, 3297.
- (40) Munzarová, M.; Kaupp, M. *J. Phys. Chem. A* **1999**, *103*, 9966.
- (41) Kutzelnigg, W.; Fleischer, U.; Schindler, M. In *Deuterium and Shift Calculation*; Springer: Berlin and Heidelberg, Germany, 1991; NMR Basic Principles and Progress Vol. 23, p 165.
- (42) Frisch, G. W.; Trucks, M. J.; Schlegel, H. B.; Scuseria, G. E.; Robb, M. A.; Cheeseman, J. R.; Scalmani, G.; Barone, V.; Mennucci, B.; Petersson, G. A.; Nakatsuji, H.; Caricato, M.; Li, X.; Hratchian, H. P.; Izmaylov, A. F.; Bloino, J.; Zheng, G.; Sonnenberg, J. L.; Hada, M.; Ehara, M.; Toyota, K.; Fukuda, R.; Hasegawa, J.; Ishida, M.; Nakajima, T.; Honda, Y.; Kitao, O.; Nakai, H.; Vreven, T.; Montgomery, J. A.; Peralta, J. E.; Ogliaro, F.; Bearpark, M.; Heyd, J. J.; Brothers, E.; Kudin, K. N.; Staroverov, V. N.; Kobayashi, R.; Normand, J.; Raghavachari, K.; Rendell, A.; Burant, J. C.; Iyengar, S. S.; Tomasi, J.; Cossi, M.; Rega, N.; Millam, J. M.; Klene, M.; Knox, J. E.; Cross, J. B.; Bakken, V.; Adamo, C.; Jaramillo, J.; Gomperts, R.; Stratmann, R. E.; Yazyev, O.;

Austin, A. J.; Cammi, R.; Pomelli, C.; Ochterski, J. W.; Martin, R. L.; Morokuma, K.; Zakrzewski, V. G.; Voth, G. A.; Salvador, P.; Dannenberg, J. J.; Dapprich, S.; Daniels, A. D.; Farkas, Ö.; Foresman, J. B.; Ortiz, J. V.; Cioslowski, J.; Fox, D. J. *Gaussian09*; Gaussian Inc., Wallingford, CT, 2009.

(43) Malkin, O. L. M. V. G.; Reviakine, R.; Arbuznikov, A. V.; Kaupp, M.; Schimmelpfennig, B.; Malkin, I.; Repisky, M.; Komorovsky, S.; Hrobarik, P.; Malkin, E.; Helgaker, T.; Ruud, K. *MAG-ReSpect, version 2.1*, 2005.

(44) Kaupp, M.; Reviakine, R.; Malkina, O. L.; Arbuznikov, A.; Schimmelpfennig, B.; Malkin, V. G. *J. Comput. Chem.* **2002**, *23*, 794.

(45) (a) Malkina, O. L.; Vaara, J.; Schimmelpfennig, B.; Munzarová, M.; Malkin, V. G.; Kaupp, M. *J. Am. Chem. Soc.* **2000**, *122*, 9206.

(b) Remenyi, C.; Reviakine, R.; Arbuznikov, A. V.; Vaara, J.; Kaupp, M. *J. Phys. Chem. A* **2004**, *108*, 5026.

(46) Becke, A. D. *Phys. Rev. A* **1988**, *38*, 3098.

(47) Perdew, J. P. *Phys. Rev. B* **1986**, *33*, 8822.

(48) Perdew, J. P. *Phys. Rev. B* **1986**, *34*, 7406.

(49) Becke, A. D. *J. Chem. Phys.* **1993**, *98*, 5648.

(50) Lee, C.; Yang, W.; Parr, R. G. *Phys. Rev. B* **1988**, *37*, 785.

(51) Stephens, P. J.; Devlin, F. J.; Chabalowski, C. F.; Frisch, M. J. *J. Phys. Chem.* **1994**, *98*, 11623.

(52) Heß, B. A.; Marian, C. M.; Wahlgren, U.; Gropen, O. *Chem. Phys. Lett.* **1996**, *251*, 365.

(53) Schimmelpfennig, A. B. *Atomic Spin-Orbit Mean-Field Integral Program*; Stockholms Universitet: Stockholm, Sweden, 1996.

(54) Hrobarik, P. *PNMR, v. 1.0*; Technische Universität Berlin, Berlin, Germany, 2011.

(55) Wolinski, K.; Hinton, J. F.; Pulay, P. *J. Am. Chem. Soc.* **1990**, *112*, 8251.

(56) Neese, F. *Inorg. Chim. Acta* **2002**, *337*, 181.

(57) Rörmelt, M.; Ye, S.; Neese, F. *Inorg. Chem.* **2008**, *48*, 784.

(58) Sinnecker, S.; Slep, L. D.; Bill, E.; Neese, F. *Inorg. Chem.* **2005**, *44*, 2245.

(59) Reed, A. E.; Curtiss, L. A.; Weinhold, F. *Chem. Rev.* **1988**, *88*, 899.

(60) Reed, A. E.; Carpenter, J. E.; Weinhold, F. *NBO Version 3.1*.

(61) Mayer, I. *Chem. Phys. Lett.* **1983**, *97*, 270.

(62) Mayer, I. *Chem. Phys. Lett.* **1985**, *117*, 396.

(63) Mayer, I. *BORDER, version 1.0*; Chemical Research Center, Hungarian Academy of Sciences, Budapest, Hungary, 2005; available from <http://occam.chemres.hu/programs>.

(64) Varetto, M. U. *Molekel, version 5.4*; Swiss National Supercomputing Center, Manno, Switzerland; available from <http://molekel.cscs.ch>.

(65) Gütlich, P.; Bill, E.; Trautwein, A. X. *Mössbauer Spectroscopy and Transition Metal Chemistry*; Springer Verlag: Berlin and Heidelberg, Germany, 2011.